

PCCP

Accepted Manuscript



This is an *Accepted Manuscript*, which has been through the Royal Society of Chemistry peer review process and has been accepted for publication.

Accepted Manuscripts are published online shortly after acceptance, before technical editing, formatting and proof reading. Using this free service, authors can make their results available to the community, in citable form, before we publish the edited article. We will replace this *Accepted Manuscript* with the edited and formatted *Advance Article* as soon as it is available.

You can find more information about *Accepted Manuscripts* in the [Information for Authors](#).

Please note that technical editing may introduce minor changes to the text and/or graphics, which may alter content. The journal's standard [Terms & Conditions](#) and the [Ethical guidelines](#) still apply. In no event shall the Royal Society of Chemistry be held responsible for any errors or omissions in this *Accepted Manuscript* or any consequences arising from the use of any information it contains.

Copper-Manganese Mixed Oxides: CO₂-selectivity, Stable, and Cyclic Performance for Chemical Looping Combustion of Methane

Pallavi Mungse,^a Govindachetty Saravanan,*^a Tomoki Uchiyama,^b Maiko Nishibori,^b Yasutake Teraoka,^b Sadhana Rayalu,^a and Nitin Labhsetwar*^a

^aEnvironmental Materials Division, CSIR-National Environmental Engineering Research Institute (CSIR-NEERI), Nehru Marg, Nagpur 440020, India.

^bDepartment of Energy and Material Sciences, Faculty of Engineering Sciences, Kyushu University, Kasuga, Fukuoka 816-8580, Japan

Author for correspondence Tel./Fax number: 91+712-2249753

E-mail address: g_saravanan@neeri.res.in
nk_labhsetwar@neeri.res.in

Abstract

Chemical looping combustion (CLC) is a key technology for oxy-fuel combustion with inherent separation of CO₂ from a flue gas, in which oxygen is derived from solid oxygen carrier. Multi-cycle CLC performance and the product selectivity towards CO₂ formation was achieved on mixed oxides of Cu and Mn (CuMn₂O₄) ($Fd\bar{3}m$, $a = b = c = 0.83$ nm) as oxygen carrier. CuMn₂O₄ was prepared by the co-precipitation method followed by annealing at 900 °C using copper (II) nitrate trihydrate and manganese (II) nitrate tetrahydrate as metal precursors. CuMn₂O₄ showed oxygen-desorption as well as its reducibility at elevated temperatures under CLC conditions. The lattice of CuMn₂O₄ was altered significantly at higher temperature, however, was reinstated virtually upon cooling in the presence of air. CuMn₂O₄ was reduced into CuMnO₂, Mn₃O₄, and Cu₂O phases at the intermediate stages, which were further reduced into metallic Cu and MnO upon the removal of *reactive oxygen* from their lattice. CuMn₂O₄ showed the remarkable activity towards methane combustion reaction at 750 °C. The reduced phase of CuMn₂O₄ containing Cu and MnO was readily reinstated when treated with air or oxygen at 750 °C, confirming efficient regeneration of oxygen carrier. Neither methane combustion efficiency nor oxygen carrying capacity was altered with increasing of CLC cycles at any tested time. The average oxygen carrying capacity of CuMn₂O₄ was estimated to be 114 mg g⁻¹, which was not altered significantly with the repeated CLC cycles. Pure CO₂ but no CO, which is one of the possible toxic by-products, was formed solely upon methane combustion reaction of CuMn₂O₄. CuMn₂O₄ shows potential as a practical CLC material both in terms of multi-cycle performance and product selectivity towards CO₂ formation.

Introduction

Anthropogenic greenhouse gas (GHG) emissions contribute significantly to the increase in global surface temperature.¹⁻⁴ Carbon dioxide (CO₂) is one of the major contributors to the GHG effect as it represents about one third of the total global anthropogenic GHG emissions.^{5,6} The enormous increase in CO₂ concentration in the atmosphere over the past few decades is due to the extensive use of the combustion processes, using fossil fuels for energy power plants, industrial as well as transportation activities, natural gas processing, etc.⁷⁻¹⁰ Fossil fuels-based power plants release about one third of the total global CO₂ emissions and therefore, great efforts have been dedicated during the last few years for its effective control.^{7,10-12} The CO₂ emissions from the power plants can be reduced significantly by (1) improving the energy efficiency, thereby emitting lesser CO₂ per unit of the fuels consumed. This is a preventive and certainly a lucrative option in terms of fuel savings, however, has several practical limitations (2) using alternative cleaner fuels (hydrogen, biodiesel etc.), which can reduce the CO₂ emissions, however, R&D to achieve these fuels are still under developmental stage and are expected to have noticeable impacts on overall energy production only after two to three decades (3) capturing and storing/sequestration of CO₂, which involves separation of CO₂ from its high volume sources and subsequent transportation followed by CO₂-sequestration.^{7,13-15} Although, capture of CO₂ seems to be viable to control the CO₂ emissions among the various proposed options, however, the separation of CO₂ from their high volume sources requires intensive energy as well as high cost. On the other hand, obtaining pure CO₂ from fossil fuels-based power plants for CO₂-sequestration would reduce the cost and energy significantly. Thus, the concentrated CO₂ can be utilized for various targeted applications with relatively less expenditure on its capture, for instance reforming reactions.¹⁶⁻¹⁹

Chemical looping combustion (CLC) is one of the emerging novel techniques with inherent tendency to separate CO₂ from a flue gas after combustion of fossil fuels for the low-cost CO₂-sequestration.²⁰⁻²⁴ CLC is a type of indirect oxy-fuel combustion process in which, oxygen is supplied by solid material for instance metal oxides, which is referred as *Oxygen Carrier*. Preliminary techno-economic assessments suggested that CLC holds a great promise for combustion processes, having the potential for achieving an efficient and low-cost CO₂ separation from the flue gas.²⁵⁻²⁷ CLC was initially explored to increase the thermal efficiency in the power generation units, however, later identified with inherent advantages of CO₂ separation, which consumes solely less energy compared to that of conventional CO₂-sequestration²⁸⁻³¹ CLC has potential for different applications, for instance clean energy generation or clean combustion, reforming,¹⁶⁻¹⁹ hydrogen production,^{32,33} etc. Moreover,

CLC has recently become promising technique for the combustion of solid fuels, for instance coal with significant advancements in coal gasification.³⁴⁻³⁶

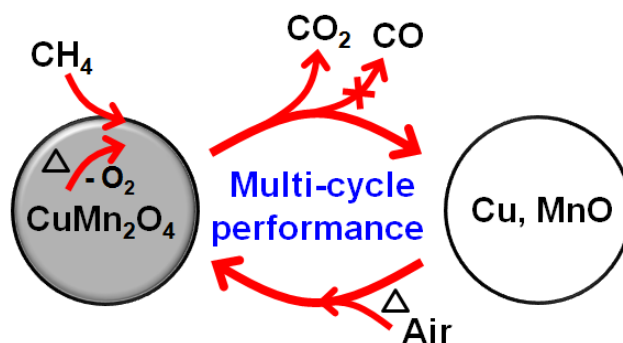
Considerable efforts have been devoted in the last few years towards the search of CLC materials in terms of the cost, performance, stability, etc. Considering the higher operational temperature as well as attrition-resistance requirements, CLC materials should have essentially higher mechanical strength to maintain the continuous and long-term CLC performance. Metal oxides of Cu, Mn, Fe, Co, and Ni have been widely explored for the CLC applications owing to their favorable reductive/oxidative thermodynamics.^{21,22,31,37} Various studies on the feasibility of these metal oxides suggest that individual metal oxides have certain practical limitations, thereby restricting their applicability towards the CLC applications³⁸⁻⁴⁵ For instance, Ni-based oxides showed the poor multi-cycle performance, carbon formation etc. that restrict their application towards CLC.⁴⁰ Fe-based oxides possess the lower oxygen carrying capacity due to their slower reduction kinetics.⁴³ Mn-based oxides showed the poor performance due to their low reactivity with the fuels.^{41,44} The lower operating temperature of Cu-based oxides hinders their utilization as oxygen carriers towards CLC due to the low melting point of Cu.^{38,39,42} Although, the above mentioned individual oxides have the limitations towards the CLC applications, however, they have certain advantages in terms of their physical and chemical properties and therefore, should be exploited for the CLC applications, especially in mixed oxide forms. Thus, it can be anticipated that mixed phases of these metal oxides may yield the better, stable CLC performance compared to that of individual oxides owing to the changes in their physicochemical and thermodynamic properties.⁴⁶⁻⁴⁸

The oxides of Cu and Mn are of particular interest due to their capability of the formation of various reductive-oxidative couples. Cu-oxides (e.g., CuO) possess the higher oxygen carrying capacity,⁴⁹ CO₂-selectivity, and both the oxidation and reduction processes of CuO are highly exothermic and thereby avoiding the need of heat supply during reduction process.⁵⁰ Moreover, Cu-oxides are relatively cheaper than most of the metal oxides, which can be used for CLC applications. Mn-based oxides have also been investigated for CLC in recent years, considering its low cost, less toxicity and favorable thermodynamic properties. Mn in the form of metal oxides usually possess the oxidation states of +2, +3, +2/+3, and +4 in the compounds of MnO, Mn₂O₃, Mn₃O₄, and MnO₂.⁵¹ The highly oxidized manganese compound, MnO₂, decomposes at about 500 °C, whereas the phase transformation from Mn₂O₃ to Mn₃O₄, which could be observed at 900 °C is of interest for CLC

applications.^{31,51} $\text{Mn}_2\text{O}_3/\text{Mn}_3\text{O}_4$ couple has the equilibrium pressure of oxygen at 899 °C, which is equal to that of the partial pressure of oxygen in air. Thus, it releases oxygen by chemical-looping combustion with oxygen uncoupling mechanism, thereby increasing the efficiency of the fuel combustion in fuel reactor.^{31,51} Therefore, long-term as well as enhanced CLC performance can be anticipated from the mixed oxides of Cu and Mn due to their unique properties by means of the oxygen storage of Cu-oxides and the thermal stability of Mn-oxides. Azad et al. reported that Cu-Mn-O spinel system and showed multi-cycle CLC performance towards CH_4 at 850 °C with maximum combustion efficiency as well as better reproducibility.⁵¹

In this study, the mixed copper and manganese oxides, CuMn_2O_4 in pure form were synthesized by co-precipitation method followed by annealing using Cu- and Mn nitrates. The formation of Cu-Mn-O phase was examined by powder X-ray diffraction (*p*XRD) technique at various annealing temperatures. Temperature controlled *p*XRD experiments were performed over CuMn_2O_4 to elucidate the changes in their lattice at elevated temperatures. The morphology of CuMn_2O_4 was observed by field emission scanning electron microscopy (FE-SEM) and transmission electron microscopy (TEM). The CLC performance of CuMn_2O_4 was evaluated using CH_4 as a fuel gas. The structures as well as the morphology of CuMn_2O_4 at the intermediate stages during CH_4 combustion as well as the products after the removal of oxygen was examined by *p*XRD, FE-SEM, and TEM. The thermally induced, spontaneous desorption of oxygen and chemically forced reduction of CuMn_2O_4 were examined by temperature programmed desorption of oxygen (O_2 -TPD) and reduction by H_2 (H_2 -TPR), respectively. Multi-cycle CLC performance of CuMn_2O_4 was examined both in terms of the CH_4 combustion efficiency as well as the oxygen carrying capacity. CO_2 -selectivity of CuMn_2O_4 was examined by monitoring of the formation of CO_2 and CO as shown in the Scheme 1.

Scheme 1. Schematic representation of multi-cycle performance and CO_2 -selectivity of CuMn_2O_4 for CLC reaction using methane as a fuel.



Experimental

Materials

Copper (II) nitrate trihydrate (99%), manganese (II) nitrate tetrahydrate (98.5%) and sodium carbonate (99.9%) were purchased from Merck India Ltd. All the chemicals were of analytical grade and used without further purification. The stock solution of 1 M Na₂CO₃ was prepared and stored for the co-precipitation of Cu- and Mn nitrates. The water used for the synthesis was purified using Elix Millipore system (BM2HA89061).

Synthesis of copper-manganese mixed oxides

Copper-manganese-based mixed oxides were prepared by co-precipitation method. Copper (II) nitrate trihydrate (0.015 mol, 3.5617 g) and manganese (II) nitrate tetrahydrate (0.03 mol, 7.3968 g) were dissolved each in 120 mL of distilled water separately. The aqueous solutions of copper nitrate were slowly added into the aqueous solutions of manganese nitrate under stirring. pH of the mixed nitrate solution was observed between 3 and 4. The aqueous solutions of these metal nitrates were heated and maintained at 80 °C till the completion of precipitation. The aqueous solution of Na₂CO₃ (1 M) was then added drop wise slowly to the aqueous solution of the mixed salts under constant stirring in order to co-precipitate the copper and manganese nitrates. The blue color of the mixed salts solution changed gradually into blackish brown, which ensures the precipitation of the metal nitrates. pH of the solution was thus turned from acidic to basic condition and maintained at pH 8 for the complete precipitation. The precipitate was left in the basic medium for 1 h without stirring and then filtered, followed by washing with distilled water. The precipitate was then dried at 120 °C for 15 h and annealed at 500, 600, 750, and 900 °C for 6 h.

Characterization

*p*XRD analysis of the samples was performed for the structural characterization in 2θ range between 10 and 80° using X-ray diffractometer (Rigaku: Miniflex-II-DD34863) using CuK α radiation ($\lambda = 0.15418$ nm) operated at 30 kV and 15 mA at a scan rate of 1° min⁻¹. Temperature controlled *p*XRD analysis of the samples was carried out using X-ray diffractometer (Rigaku: Ultima IV) using CuK α radiation operated at 30 kV and 40 mA to study the lattice strains. The samples were heated from 30 to 750 °C at the ramping rate of 10° min⁻¹ under the flow of N₂ and periodically recorded the *p*XRD

profiles at various temperatures, where the partial pressure of oxygen, $p(\text{O}_2)$, as residual impurity was estimated in the $p\text{XRD}$ sampling compartment to be 0.15 %. The material was then cooled down to room temperature in the presence of air and $p\text{XRD}$ profile was again recorded at 50 and 25 °C. FE-SEM observation of the samples was carried out using JEOL instrument (JSM-6340F) operated at the acceleration voltage of 10.0 kV to observe the morphology of the samples. TEM observation of the samples was carried out using JEOL JEM-1400 instrument operated at the acceleration voltage of 120 kV. The samples were dispersed in methanol and carefully dropped on carbon coated Cu-grids. O_2 -TPD and H_2 -TPR of the samples were measured using a BEL-CAT instrument (BEL-CAT, BEL Japan). The instrument was equipped with a thermal conductivity detector (TCD) to estimate the changes in the concentration of O_2 and H_2 in the gas streams. For both O_2 -TPD and H_2 -TPR experiments, the flow rate of a gas stream and temperature ramping rate was maintained at 30 mL min^{-1} and 10 °C min^{-1} , respectively. For O_2 -TPD analysis, the sample was pretreated at 400 °C in the presence of air stream for 30 min followed by cooling down to 50 °C. The temperature of the sample then increased up to 950 °C in the presence of He. For H_2 -TPR analysis, the samples were pretreated in air stream at 200 °C for 2 h followed by cooling down to 50 °C. The samples were then heated up to 700 °C in the presence of N_2 -balanced H_2 (5%) stream.

Evaluation for oxygen carrying capacity

The CLC performance of the samples was evaluated in a fixed-bed, quartz reactor equipped with a thermocouple in contact with the sample bed and using 2.5 and 5 % of CH_4 as fuel balanced with He. Prior to the evaluation, the powdered form of the samples were made into the small pellets and then rubbed on the sieve having the mesh size of 1 mm to yield homogeneous granular samples. 1 g of the granular samples was sandwiched between quartz wool inside the quartz column and the temperature was controlled using a temperature-controlled tubular furnace. The experimental set up consisted of mass flow controllers (Alborg, USA), gas chromatograph (Shimadzu GC-2014) and a mixing chamber. The samples were pre-treated at 200 °C for 30 min in prior to the CLC evaluation under the He environment to remove any pre-adsorbed impurities and the residual air. The samples were then heated to 750 °C and 2.5 or 5 % of CH_4 balanced with He was subjected through the samples at a flow rate of 10 mL min^{-1} . Pure CH_4 was not intentionally used for the CLC evaluation owing to get sufficient break through time, which can eliminate the possible measurement errors in break-through curves. The effluent stream from the reactor containing various gas components was continuously

analyzed by an online gas chromatograph equipped with a thermal conductivity detector using porapak Q (Supelco, Product Code - 12469) and the molecular sieve 5A (Restek, product code – 80473-850) columns. Multi-cycle CLC performance of the samples was further investigated by repeating the reduction and re-oxidation cycles. Prior to the multi-cycle CLC performance, the reduced copper and manganese samples were re-oxidized in the presence of air for 1 h at 750 °C. The residual air was removed by flushing of He gas in the reactor. Four consecutive reduction and re-oxidation cycles were performed to evaluate multi-cycle CLC performance. The oxygen carrying capacity of the samples was evaluated by the sum of the oxygen is required for methane conversion, which was calculated by the ratio of the total and un-reacted CH₄ per sampling time, 1.5 min.

Results and discussion

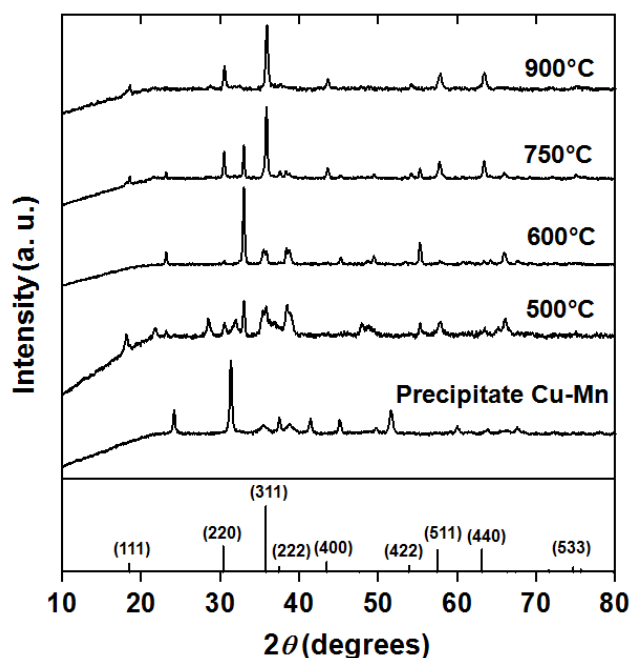


Figure 1. *p*XRD profiles for the precipitate obtained from Cu- and Mn-nitrates and the products obtained after annealing at various temperatures. The simulated XRD lines for pure CuMn₂O₄ are shown as reference.

The formation of mixed oxides of Cu and Mn was examined by annealing of the precipitate that was obtained from the co-precipitation of Cu- and Mn nitrates followed by oven drying. Figure 1 represents the *p*XRD profiles of the precipitate and the products obtained at various annealing temperatures. The precipitate showed the characteristic sharp peaks at 24.2°, 31.3°, 37.5°, 41.4°, 45.1°, 51.6°, 60.1°, 63.8°, and 67.7° for the reflection planes of (012), (104), (110), (113), (202), (116), (122),

(214), and (300) respectively, which correspond to MnCO_3 ($R\bar{3}c$, $a = b = 0.47$ nm; $c = 1.56$ nm). In addition, the precipitate also showed the broad peaks at 35.5° and 38.7° for the reflection planes of (11 $\bar{1}$) and (111) respectively, which correspond to CuO ($C2/c$, $a = 0.46$ nm; $b = 0.34$ nm; $c = 0.51$ nm). The co-precipitation of Cu- and Mn nitrates using Na_2CO_3 followed by oven drying yielded the physical mixture of MnCO_3 and CuO . In addition to the characteristic peaks of CuO , the products obtained after annealing at 500°C showed the characteristic peaks at 23.1° , 32.9° , 38.2° , 55.1° , and 65.7° for the reflection planes of (211), (222), (400), (440), and (622) respectively, which correspond to Mn_2O_3 ($Ia\bar{3}$, $a = b = c = 0.94$ nm). Also, the characteristic peaks at 18.1° , 28.7° , 30.8° , 31.1° , 31.5° , 31.8° , 36.3° , 38.2° , 47.8° , 57.9° , and 66.1° for the reflection planes of (200), (111), (201), (020), ($\bar{3}11$), ($\bar{2}20$), ($\bar{2}21$), ($\bar{4}21$), (421) and ($\bar{2}23$) respectively, corresponding to Mn_5O_8 ($C2/m$, $a = 1.03$ nm; $b = 0.57$ nm; $c = 0.48$ nm) were also obtained. The precipitate annealed at 600°C formed solely the physical mixture of Mn_2O_3 and CuO . MnCO_3 in the precipitate was decomposed into Mn_2O_3 and Mn_5O_8 at 500°C and solely into Mn_2O_3 at 600°C . The precipitate annealed at 750°C showed the characteristic peaks for Mn_2O_3 and the mixed oxides of Cu and Mn, CuMn_2O_4 ($Fd\bar{3}m$, $a = b = c = 0.83$ nm) as observed at 18.4° , 30.3° , 35.7° , 37.3° , 43.4° , 53.8° , 57.4° , 63° , and 74.6° for the reflection planes of (111), (220), (311), (222), (400), (422), (511), (440), and (533) respectively. These results infer that the solid-state reaction between Mn_2O_3 and CuO were occurred at 750°C and therefore Cu-Mn-O phase (CuMn_2O_4) was formed. The products obtained after annealing the precipitate at 900°C showed solely the characteristic peaks for CuMn_2O_4 (designated hereafter as CM).⁵² These results suggest that the physical mixture of Cu- and Mn oxides were formed from the precipitate between 500° and 600°C and the mixed oxides were obtained through solid-state reaction at 750°C . CuMn_2O_4 phase was achieved without forming any by-products or impurities at 900°C from the precipitate of Cu- and Mn-nitrates.

Figure 2a shows the FE-SEM image of CM having the particles of various sizes and shapes including octahedral structures. The particle size of CM is of the order of several micrometers due to the agglomeration of the particles at higher synthesis temperature. In addition, the tubular structures were also formed on the dense surfaces of CM marked as arrows in the image. The TEM image of CM shows the tubular structure having several hundreds of nm in length and ~ 70 nm in diameter (Figure 2b). The thickness of the wall of CM ranged between 10 and 15 nm.

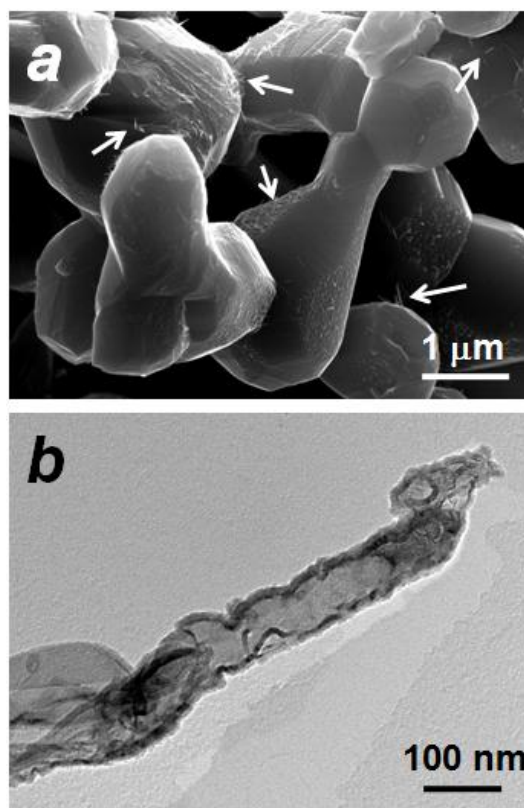


Figure 2. FE-SEM (a) and TEM (b) images of CuMn_2O_4 .

Temperature controlled p XRD analysis of CM was performed at various temperatures in order to understand the changes in the lattice at elevated temperatures. It has been reported that the lattice of oxide materials would induce the strains in their lattice, which is strongly dependent on the temperatures.^{53,54} Therefore, the dependence of lattice constant of CM at various temperatures would give the essential information about the possibility to utilize them for CLC reaction. CM was heated from room temperature to 750 °C in the presence of N_2 and performed p XRD analysis periodically to observe the changes in the lattice. Figure 3a shows the p XRD profiles at various temperatures in the presence of N_2 and air. CM showed a characteristic peak at 35.7° for the reflection plane of (311), which was shifted progressively to the lower diffraction angles with increasing temperature and observed at 35.2° at 750 °C in the presence of N_2 . Interestingly, the peak position of the reflection plane of (311) was retained virtually when CM was cooled down to 25 °C in the presence of air. These results indicate that the lattice of CM is most likely altered upon heating and cooling of CM in the presence of N_2 and air. It was ensured, however, that the structure of CM was not decomposed upon heating in the presence of N_2 , as shown in the supporting information (Figure S1). As can be seen in more detail in Figure 3b, the lattice constant of CM ($a = 0.8317$ nm at 30 °C) was gradually increased

with increasing of temperature up to 300 °C and then steeply increased between 300 and 400 °C. The lattice constant further increased progressively with increasing of temperature and reached to 0.8450 nm at 750 °C. The lattice constant was virtually retained again to their original value upon cooled down to room temperature in the presence of air. The observed trend is consistent with the reported results of mixed oxides.⁵⁵ It has been reported that CuMn_2O_4 exists two ionic configurations of $\text{Cu}^+[\text{Mn}^{3+}\text{Mn}^{4+}]\text{O}_4$ and $\text{Cu}^{2+}[\text{Mn}^{3+}_2]\text{O}_4$ as low and high temperature ionic configuration, respectively.⁵⁶ The transformation of low-temperature ionic configuration in to the high-temperature ionic configuration can be observed at 328 °C, which may likely induce the changes in the lattice of CM. The steep enhancement in the lattice constant between 300 and 400 may be ascribable the change from low-temperature to high temperature ionic configuration upon heating.

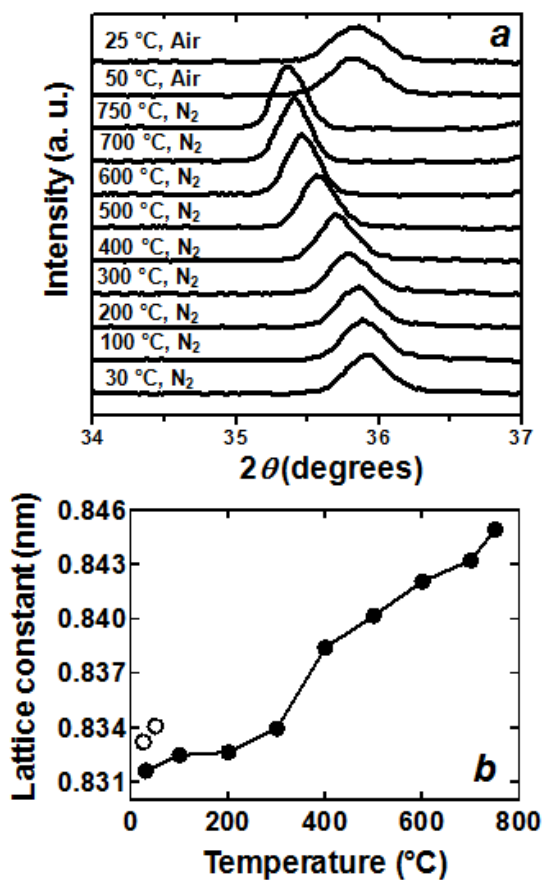


Figure 3. (a) Temperature controlled p XRD profiles of CuMn_2O_4 at various temperatures in the presence of N_2 and air (b) The dependence of lattice constant of CuMn_2O_4 as a function of temperature. CuMn_2O_4 was heated in the presence of N_2 (closed circle) up to 750 °C and cooled down to 25 °C in the presence of air (open circle).

The redox behavior of CM is an important property to discuss its CLC performance. Therefore, the thermally induced, spontaneous desorption of oxygen and chemically forced reduction were examined by O₂-TPD and H₂-TPR, respectively (Figure 4). The O₂-TPD profile (Figure 4a) shows two desorption peaks at 555 and 765 °C with desorption amounts of 0.061 and 0.295 mol-O₂ mol-CM⁻¹, respectively. CM after O₂-TPD experiments was analyzed by *p*XRD that showed a mixture of Mn₃O₄ and CuMnO₂ (Figure S2), and therefore the following reaction was most likely occurred during the desorption of oxygen from CM; $\text{CuMn}_2\text{O}_4 \rightarrow \text{CuMnO}_2 + 1/3\text{Mn}_3\text{O}_4 + 1/3 \text{O}_2$. According to the reaction, the amount of desorbed oxygen is to be 0.33 mol-O₂ mol-CM⁻¹, which is reasonably closer to the sum of two desorption peaks (0.356 mol-O₂ mol-CM⁻¹). The reason, why two desorption peaks were observed is not clear, however, one possibility is that nano-tubular and well-crystallized CM may get decomposed at lower and higher temperature, respectively (Figure 2). Overall, TPD results indicate tendency of CM to loose oxygen at higher temperatures.

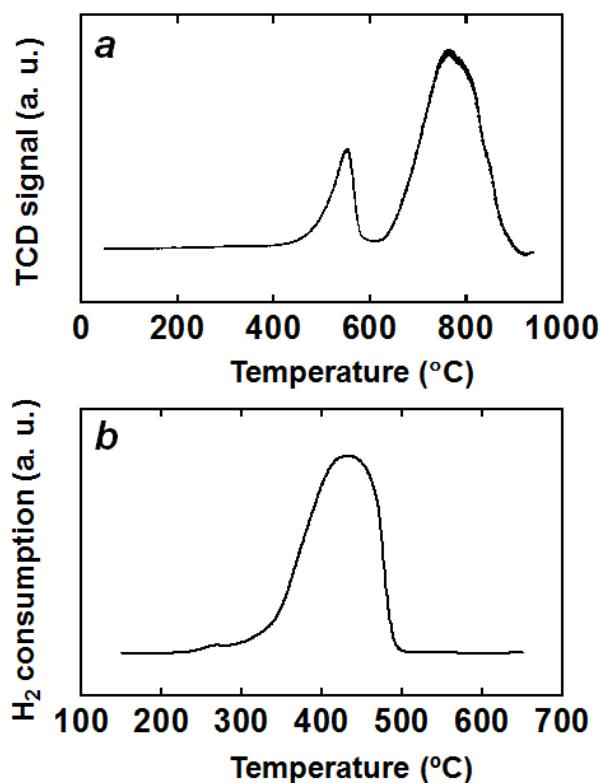


Figure 4. O₂-TPD (a) and H₂-TPR (b) profiles of CuMn₂O₄.

H₂-TPR experiments were also performed over CM to investigate their reduction behavior (Figure 4b). CM showed a characteristic peak with high intensity in the region of 250 and 500 °C

centered at 440 °C due to the reduction of oxygen released from CM. The consumption of H₂ was calculated by the integration of the peak is to be 2.2 mol-H₂ g⁻¹, which is reasonably closer to the stoichiometry of the reduction reaction of CM; $\text{CuMn}_2\text{O}_4 + 2 \text{H}_2 \rightarrow \text{Cu}(0) + 2\text{MnO} + 2 \text{H}_2\text{O}$. The formation of metallic Cu and MnO as the final products was confirmed after reduction of CM by methane through CLC reaction (see Figure 6 for the details).

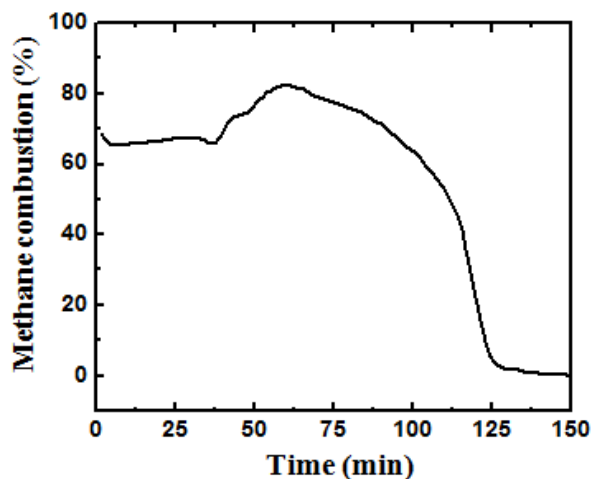


Figure 5. The CH₄ combustion efficiency of CuMn₂O₄ as a function of time.

The CH₄ combustion efficiency of CM was evaluated through combustion reaction at 750 °C using a fixed bed reactor. The oxygen from CM as *oxygen carrier* reacts with CH₄ to form pure CO₂. Figure 5 represents the CH₄ combustion efficiency as a function of time. Approximately 70% of the CH₄ combustion efficiency was achieved solely up to 40 min by CM at the earlier stages. 100% CH₄ combustion efficiency, however, was not realized due to the higher quantity of CH₄ in the stream or relatively insufficient amounts of CM material to release more oxygen. The un-reacted CH₄ was confirmed in the effluent stream from the outlet of the reactor, as shown in the supporting information (Figure S3). Interestingly, 100% CH₄ combustion efficiency was realized when the concentration of CH₄ in the stream reduced into half (2.5 %) of their original concentration (Figure S4). It should be noted that the CH₄ combustion efficiency increased steadily with increasing time and reached up to 80% at 54 min. The enhancement in the CH₄ combustion efficiency after 40 min was due to the formation of intermediates of CuMnO₂ (Figure S5) of CM which can likely release the oxygen more effectively at 750 °C. The CH₄ combustion efficiency decreased progressively at the later stages with increasing time and reached virtually 0% at 150 min due to the exhaustion of *reactive* oxygen from CM, i.e., CM become reduced phase under the present reaction condition (designated as CMR).

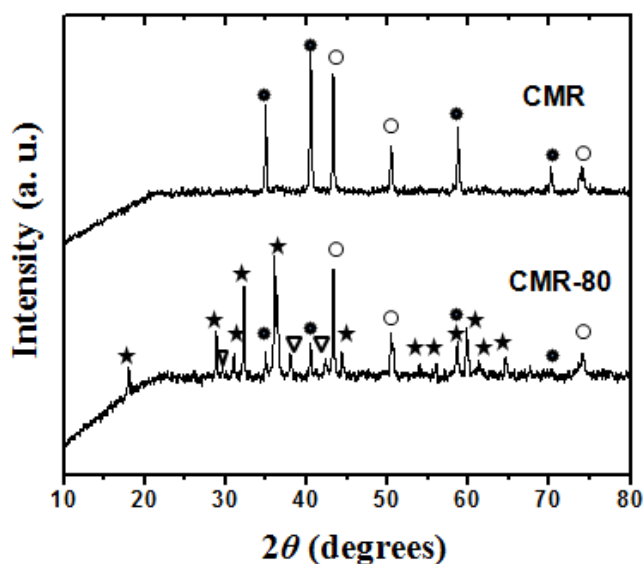


Figure 6. *p*XRD profiles for the intermediate products at 80 min and the reduced products of CH₄ combustion reaction on CuMn₂O₄. Mn₃O₄ (★), Cu (○), MnO (●), Cu₂O (▽).

*p*XRD analysis were performed further to identify the structures of CM at the intermediate stages at 20 (Figure S5) and 80 min and CMR. The CH₄ combustion reaction was intentionally terminated at 80 min and the materials were recovered to perform *p*XRD analysis to identify the intermediate products. Figure 6 shows the *p*XRD profiles for the intermediate products at 80 min and CMR. The *p*XRD profile for the intermediate products showed the characteristic peaks for the oxides of Cu and Mn as well as Cu-metal. The intermediate products showed the characteristic peaks at 18°, 28.9°, 31°, 32.3°, 36°, 36.4°, 44.4°, 50.7°, 58.5°, 59.8°, 64.6°, and 74.1° for the reflection planes of (101), (112), (200),(103), (211), (202), (220), (105), (321), (224), (400), and (413) respectively, which correspond to Mn₃O₄ (*I4*₁/*amd*, *a* = *b* = 0.57 nm; *c* = 0.94 nm) and also showed the characteristic peaks for Cu₂O (*Pn* $\bar{3}$ *m*, *a* = *b* = *c* = 0.42 nm) observed at 29.6°, 36.5°, 42.4°, and 61.5° for the reflection planes of (110), (111), (200), and (220) respectively. Moreover, the intermediate products showed the characteristic peaks at 34.9°, 40.5°, and 58.6° for the reflection planes of (111), (200), and (220) respectively, which correspond to MnO (*Fm* $\bar{3}$ *m*, *a* = *b* = *c* = 0.44 nm). The characteristic reflection peaks for Cu-metal (*Fm* $\bar{3}$ *m*, *a* = *b* = *c* = 0.36 nm) was also observed from the intermediate products at 43.2°, 50.4°, and 74.1° for the reflection planes of (111), (200), and (220) respectively. *p*XRD analysis of CMR revealed the characteristic sharp reflection peaks for MnO and Cu-metal, indicating that MnO and Cu-metal are the final products after releasing of oxygen from CM. It should be noted that MnO

was not reduced further to form Mn-metal due to the thermodynamic limitations. MnO is a very stable phase having higher free energy of formation (ΔG_f) of 104 Kcal mole⁻¹. This is a distinct advantage of present Cu-Mn based oxygen carrier, since MnO can provide structural stability to the reduced CMR phase, as many single metal oxide based oxygen carriers show inferior structural stability on reduction to metallic state. Therefore, *p*XRD results at various stages of the CLC reaction suggest that CM was reduced in to CuMnO₂ and Mn₃O₄ during the earlier stage of CLC through the reaction of $\text{CuMn}_2\text{O}_4 \rightarrow \text{CuMnO}_2 + 1/3\text{Mn}_3\text{O}_4 + 1/3 \text{O}_2$. However, a mixture of CuMnO₂ and Mn₃O₄ was reduced further in to MnO and Cu(0) through the reaction of $\text{CuMnO}_2 + 1/3\text{Mn}_3\text{O}_4 \rightarrow \text{Cu}(0) + \text{MnO} + 2/3 \text{O}_2$ in the later stage of CLC. The consumption of oxygen during the initial stage of methane combustion (up to 40 min) was about one third of the total consumption (Figure 5). Therefore, an increase in CH₄ combustion efficiency after 40 min is most likely due to the decomposition of CuMnO₂ that formed metallic Cu and MnO.

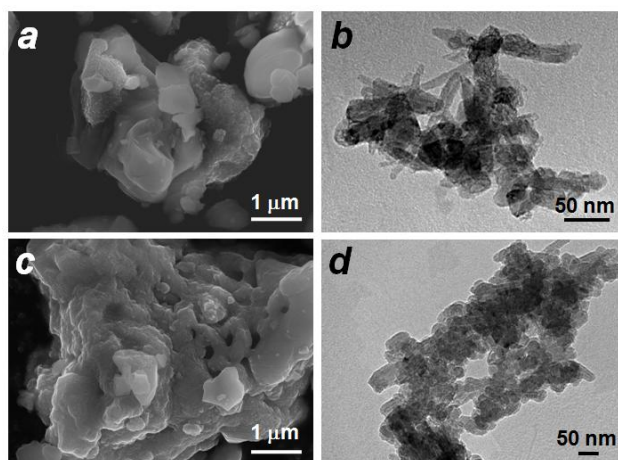


Figure 7. FE-SEM images of the intermediate products at 80 min (*a*) and the reduced products (*c*). TEM images of the intermediate products at 80 min (*b*) and the reduced products (*d*).

FE-SEM observation over CMR-80, samples recovered at 80 min of reduction and CMR after four successive reduction and re-oxidation cycles was performed to study the changes in their morphology. The large-sized particles of CM (Figure 2*a*) were decomposed after 80 min of reduction due to the decomposition of CM into the metal oxides and metal as shown in Figure 7*a*. The dense surface of the materials can also be observed due to the incomplete reduction (i.e., removal of *reactive* oxygen) at 80 min. The TEM image of CMR-80 showed the particles having tubular and semi-spherical structures (Figure 7*b*). The long tubular structure of CM (Figure 2*b*) is decomposed into the small tubular and semi-spherical structures. Figure 7*c* shows the FE-SEM image of CMR after complete

removal of *reactive* oxygen from CM. The dense and smooth surface of CM was almost completely changed due to the removal of *reactive* oxygen and the particles of CM were agglomerated at 750 °C. Figure 7d shows the TEM image of CMR. The dense surfaces of CM were further decomposed into spherical shaped particles as a result of the complete removal of *reactive* oxygen. The tubular structure was no longer observed due to the complete decomposition of CM.

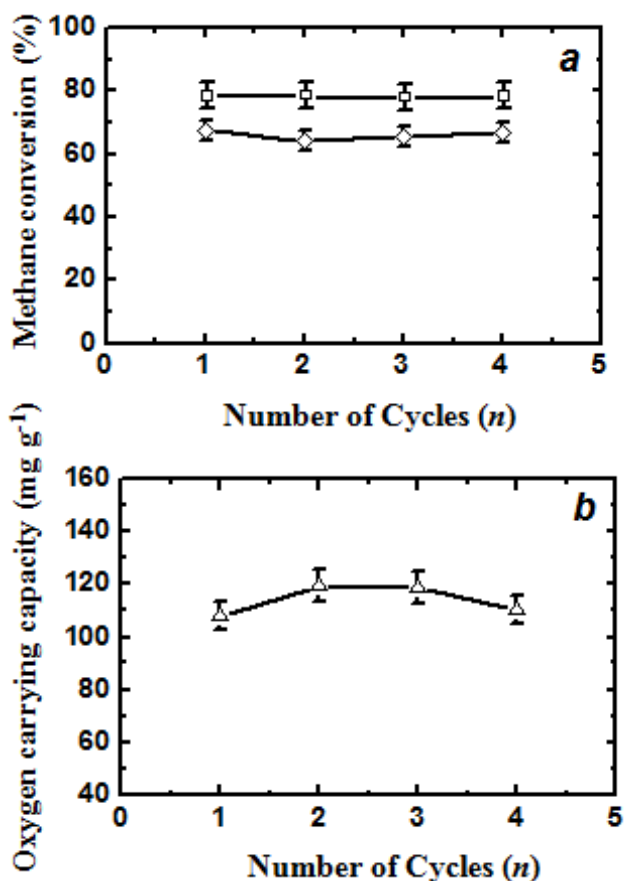


Figure 8. Multi-cycle performance of CuMn₂O₄. (a) CH₄ combustion efficiency as a function of cycles (*n*) at two different time interval of 30 min (◇) and 75 min (□). (b) oxygen carrying capacity as a function of cycles (*n*).

Multi-cycle CLC performance was examined for CM material, which is one of the essential requirements to realize the practical CLC materials. CMR was re-oxidized in the presence of air at 750 °C (designated as CMO hereafter). The formation of Cu-Mn-O phase of CuMn₂O₄ and the morphological structures of CMO after re-oxidation were confirmed by *p*XRD analysis and FE-SEM (Figure S6). The *p*XRD pattern of CMO (Figure S6a) was virtually consistent with that of CM (CuMn₂O₄), confirming the regeneration of CM by the air treatment at 750 °C. Multi-cycle CLC

performance of CM was evaluated in terms of the CH₄ combustion efficiency as well as the oxygen carrying capacity. CM was subjected to four successive reduction and re-oxidation cycles and both the CH₄ combustion efficiency (Figure S7) and the oxygen carrying capacity were estimated at 750 °C using 5% CH₄ as fuel. The observed CH₄ combustion efficiency trends are virtually same indicating their inherent behavior of CM. Figure 8a shows the CH₄ combustion efficiency at 30 min and 75 min as a function of number of cycles, which showed the constant and the stable CLC performance. The CH₄ combustion efficiency of CM is estimated to be 67% and 80% at 30 and 75 min, respectively for 1st cycle, which is retaining almost the same efficiency for the successive cycles at any tested time. The oxygen carrying capacity of CM for 1st cycle was also estimated to be 107.79 mg g⁻¹ which is again retaining almost the same capacity for the successive cycles within the error limit as shown in Figure 8b. The calculated average oxygen carrying capacity of CM is to be 114 mg g⁻¹ which is approximately 85% of the theoretical oxygen carrying capacity (134.9 mg g⁻¹) of the CLC reaction of CM. The small loss of oxygen carrying capacity than that of its theoretical value is due to likely the removal of reactive oxygen from CM during heating of CM up to 750 °C before methane combustion reaction. It should be noted that the oxides of Cu and Mn release oxygen through chemical-looping combustion with oxygen uncoupling mechanism.^[51] Unambiguously, these results suggest that CM possesses the stable CLC performance and shows good potential as a practical material for the CLC applications.

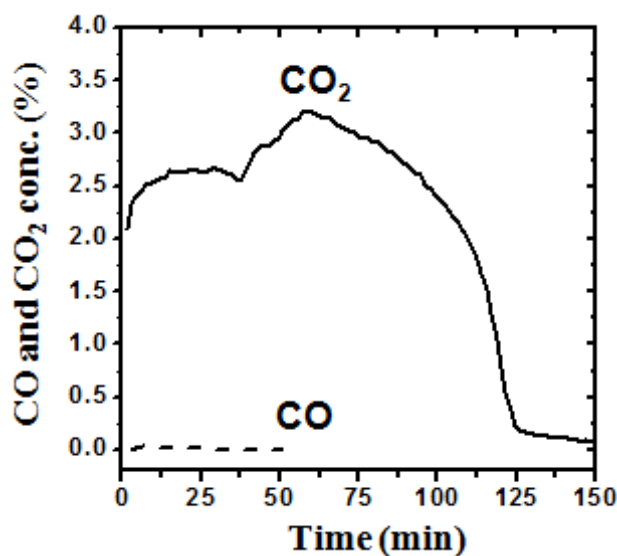


Figure 9. The dependence of the formation of CO and CO₂ of methane combustion reaction on CuMn₂O₄.

The formation of pure CO_2 from oxygen carrier is one of the essential requirements to realize them as practical oxygen carrier for the CLC applications. Therefore, the selectivity of CM towards the formation of CO and CO_2 was also examined during CH_4 combustion reaction. Figure 9 represents the selectivity of CM towards the formation of CO and CO_2 as a function of time. CO_2 was formed solely from CM with increasing of reaction time. It should be noted that the trend for CO_2 formation of CM is consistent with the CH_4 combustion efficiency trend (Figure 5). Surprisingly, no CO, which is one of the possible toxic by-products was formed during CH_4 combustion reaction as shown in the Figure 9. These results suggest that CM possesses high selectivity towards the formation of CO_2 upon CH_4 combustion reaction.

Conclusion

The mixed oxide of Cu and Mn, CuMn_2O_4 , was prepared through co-precipitation method followed by annealing at $900\text{ }^\circ\text{C}$ using the nitrate salts of Cu and Mn as the precursors. CuMn_2O_4 showed high activity towards methane combustion reaction. The lattice constant of CuMn_2O_4 increased significantly with increasing temperature, however, can be virtually retained after re-oxidation of reduced- CuMn_2O_4 . CuMn_2O_4 was partially reduced into Mn_3O_4 and Cu_2O phases at the intermediate stages and further reduced into metallic Cu and MnO upon complete removal of *reactive oxygen*. The dense solid surface of CuMn_2O_4 was decomposed into small-sized particles due to the removal of oxygen and further agglomerated at elevated temperatures. The reduced CuMn_2O_4 phase containing Cu and MnO can be readily reinstated by treating at $750\text{ }^\circ\text{C}$ in the presence of air. CuMn_2O_4 showed the stable multi-cycle CLC performance in which, the methane combustion efficiency is not altered with increasing of CLC cycles at any tested time. No significant changes in the oxygen carrying capacity of CuMn_2O_4 were observed with increasing of CLC cycles. Moreover, CuMn_2O_4 showed the product selectivity towards CO_2 formation. Pure CO_2 was solely formed during methane combustion reaction of CuMn_2O_4 . CuMn_2O_4 may be utilized as the practical materials for CLC applications. Formation of thermodynamically stable MnO phase on reduction of CuMn_2O_4 under CLC conditions with its chemical compatibility to Cu metal to get re-oxidized in to original phase, as well high reactivity with methane makes this binary oxide system very potential for CLC applications.

Electronic Supplementary Information (ESI) available: [Temperature-controlled *p*XRD profiles of CuMn₂O₄; *p*XRD profile of CuMn₂O₄ after O₂-TPD experiments; Time dependence of un-reacted methane in the effluent stream of the outlet of the reactor; CH₄ combustion efficiency for CuMn₂O₄ at the concentration of 2.5 % of CH₄; *p*XRD profile of the intermediate product at 20 min; *p*XRD profile and FE-SEM images of re-oxidized CuMn₂O₄; Multi-cycle CH₄ combustion performance of CuMn₂O₄.]. See DOI: 10.1039/b000000x/

Acknowledgement

The authors thank Department of Science and Technology (project No. G-1-1749) for financial support as well as Council of Scientific and Industrial Research (CSIR), Govt. of India (project No. CSC0102) for part financial support. The authors thank Dr. Fabien Grasset and Dr. Chrystelle Neaime, University of Rennes, France and Dr. Liu Haidi, Kyushu University, Japan for the material characterization studies. The authors also thank Dr. Satish R. Wate, the Director, CSIR-NEERI for the laboratory support to these projects.

References

-
- 1 M. Halmann and M. Steinberg, Greenhouse Gas Carbon Dioxide Mitigation: Science and Technology. Lewis Publishers, Boca Raton, FL, USA, 2000.
 - 2 Intergovernmental Panel on Climate Change (IPCC). Climate Change 2001, Cambridge University Press: New York, 2001.
 - 3 Intergovernmental Panel on Climate Change (IPCC), Climate Change 2007, Cambridge University Press: Cambridge, 2007.
 - 4 Intergovernmental Panel on Climate Change (IPCC), Climate Change 2013, Summary for Policymakers.
 - 5 H. Houghton, Global Warming. The Complete Briefing. Third Edition. Cambridge University Press: New York, 2004.
 - 6 J. G. J. Olivier, G. Janssens-Maenhout, M. Muntean and J. A. H. W. Peters, Trends in Global CO₂ Emissions, PBL Netherlands Environmental Assessment Agency, The Hague, 2013.
 - 7 Intergovernmental Panel on Climate Change (IPCC) Special Report on Carbon Dioxide Capture and Storage, 2005.

-
- 8 U.S. Environmental Protection Agency Inventory of U.S. Greenhouse Gas Emissions and Sinks 1990-2005; Environmental Protection Agency: Washington, DC, 2007.
 - 9 F. Zeman and M. Castaldi, *Environ. Sci. Technol.*, 2008, **42**, 2723-2727.
 - 10 M. V. Hoeven, IEA statistics, CO₂ Emissions from fuel combustion: Highlights, 2012
<http://data.iea.org>.
 - 11 A. Abad, T. Mattisson, A. Lyngfelt and M. Ryden, *Fuel*, 2006, **85**, 1174-1185.
 - 12 Environmental Protection Agency. Standards of Performance for Greenhouse Gas Emissions for New Stationary Sources: Electric Utility Generating Units. Federal Register / Vol. 77, No. 72 / Friday, April 13, 2012 / Proposed Rules.
 - 13 H. J. Herzog, New technologies could reduce carbon dioxide emissions to the atmosphere while still allowing the use of fossil fuels. *Environ. Sci. Technol.*, 2001.
 - 14 Carbon Sequestration Technology Roadmap and Program Plan; U.S. Department of Energy, 2007.
 - 15 Carbon Capture and Storage: Progress and Next Steps. IEA/CSLF Report to the Muskoka 2010 G8 Summit.
 - 16 L. Tian, X. H. Zhao, B. S. Liu and W. D. Zhang, *Energ. Fuel*, 2009, **23**, 607-612.
 - 17 S. Y. Foo, C. K. Cheng, T. H. Nguyen and A. A. Adesina, *Ind. Eng. Chem. Res.*, 2010, **49**, 10450-10458.
 - 18 M. Najera, R. Solunke, T. Gardner and G. Vesper, *Chem. Eng. Res. & Des.*, 2011, **89**, 1533-1543.
 - 19 J. M. Bermudez, N. Ferrera-Lorenzo, S. Luque, A. Arenillas and J. A. Menendez, *Fuel Process Technol.*, 2013, **115**, 215-221.
 - 20 M. Ishida, D. Zheng and T. Akehata, *Energy*, 1987, **12**, 147-154.
 - 21 M. M. Hossain and H. I. De Lasa, *Chem. Eng. Sci.*, 2008, **63**, 4433-4451.
 - 22 H. Fang, Li. Haibin and Z. Zengli, *Int. J. Chem. Eng.*, 2009, doi:10.1155/2009/710515.
 - 23 B. Moghtaderi, *Energ. Fuel*, 2012, **26**, 15-40.
 - 24 L. S. Fan, L. Zeng, W. Wang and S. Luo, *Energ. Environ. Sci.*, 2012, **5**, 7254-7280.
 - 25 W. K. Lewis, E. R. Gilliland and M. P. Sweeney, *Chem. Eng. Prog.*, 1951, **47**, 251-256.
 - 26 W. K. Lewis and E. R. Gilliland, Production of pure carbon dioxide. U. S. Patent 2, 665, 972, 1954.
 - 27 M. Ishida and H. Jin, *Energy* (Oxford, United Kingdom) 1994, **19**, 415-422.
 - 28 M. Ishida and H. Jin, *Energ. Convers. Manage.*, 1997, **38**, 187-192.
 - 29 L. S. Fan, Chemical Looping Systems for Fossil Fuel Conversions; John Wiley and Sons: New York, 2010; ISBN: 978-0-470-87252-9.

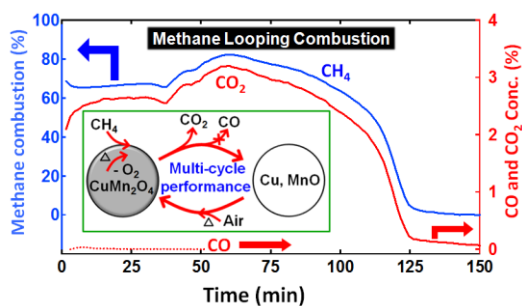
-
- 30 A. Lyngfelt and T. Mattisson, *Materials for chemical-looping combustion*. Weinheim: WILEY-VCH Verlag GmbH & Co. KGaA; 2011.
- 31 J. Adanez, A. Abad, F. Garcia-Labiano, P. Gayan and L.F. De Diego, *Prog. Energ. Combust.*, 2012, **38**, 215–282.
- 32 S. Chen, Z. Xue, D. Wang and W. Xiang, *Int. J. of Hydrogen Energ.*, 2012, **37**, 8204-8216.
- 33 M. Ortiz, P. Gayán, L. F. De Diego, F. García-Labiano, A. Abad, M. A. Pans and A. Adánez, *J. Power Sources*, 2011, **196**, 4370-4381.
- 34 T. Mattisson, A. Lyngfelt and H. Leion, *Int. J. Greenh. Gas Con.*, 2009, **3**, 11-19.
- 35 P. Markstrom, C. Linderholm and A. Lyngfelt, *Int. J. Greenh. Gas Con.*, 2013, **15**, 150-162.
- 36 A. Lyngfelt, *Appl. Energ.*, 2014, **113**, 1869-1873.
- 37 P. Cho, T. Mattisson and A. Lyngfelt, *Fuel*, 2004, **83**, 1215–2125.
- 38 T. Mattisson, M. Johansson and A. Lyngfelt, *Energ. Fuel*, 2003, **17**, 643-651.
- 39 L. F. De Diego, F. Garcia-Labiano, J. Adanez, P. Gayan, A. Abad, B. M. Corbella and J. M. Palacios, *Fuel*, 2004, **83**, 1749–1757.
- 40 P. Cho, T. Mattisson and A. Lyngfelt, *Ind. Eng. Chem. Res.*, 2005, **44**, 668–676.
- 41 S. Roux, A. Bensakhria and G. Antonini, *Int. J. Chem. React. Eng.*, 2006, **4**, 38.
- 42 E. Jerndal, T. Mattisson and A. Lyngfelt, *Chem. Eng. Res. Des.*, 2006, **84**, 795–806.
- 43 A. Abad, J. Adanez, F. Garcia-Labiano, L. F. De Diego, P. Gayan and J. Celaya, *Chem Eng. Sci.*, 2007, **62**, 533-549.
- 44 R. Siriwardane, H. Tian, G. Richards, T. Simonyi and J. Poston, *Energ. Fuel*, 2009, **23**, 3885-3892.
- 45 B. Moghtaderi and H. Song, *Energ. Fuel*, 2010, **24**, 5359-5368.
- 46 H. Jin, T. Okamoto and M. Ishida, *Energ. Fuel*, 1998, **12**, 1272-1277.
- 47 G. Azimi, H. Leion, M. Ryden, T. Mattisson and A. Lyngfelt, *Energ. Fuel*, 2013, **27**, 367-377.
- 48 R. Siriwardane, H. Tian, T. Simonyi and J. Poston, *Fuel*, 2013, **108**, 319-33.
- 49 F. Garcia-Labiano, L. F. De Diego, J. Adanez, A. Abad and P. Gayan, *Ind. Eng. Chem. Res.*, 2004, **43**, 8168-8177.
- 50 L. F. De Diego, F. Garcia-Labiano, P. Gayan, J. Celaya, J. M. Palacios and J. Adanez, *Fuel*, 2007, **86**, 1036-1045.
- 51 A. M. Azad, A. Hedayati, M. Ryden, H. Leion and T. Mattisson, *Energy Technol.*, 2013, **1**, 59-69.
- 52 A. P. B. Sinha, N. R. Sanjana and A. B. Biswas, *J. Phys. Chem.*, 1958, **62**, 191–194.

-
- 53 G. K. Bichile and R.G. Kulkarni, *J. Phys. C: Solid State Phys.*, 1975, **8**, 3988-3992.
- 54 A. J. Saldivar-Garcia and H. F. Lopez, *Metallurgical and Materials Transactions A*, 2004, **35A**, 2517-2533.
- 55 B. P. Mandal, R. Shukla, S. N. Achary and A. K. Tyagi, *Inorg. Chem.*, 2010, **49**, 10415-10421.
- 56 D. B. Ghare, A. P. B. Sinha and L. Singh, *J. Mater. Sci.*, 1968, **3**, 389-394.

Table of contents

Copper-Manganese Mixed Oxides: CO₂-selectivity, Stable, and Cyclic Performance for Chemical Looping Combustion of Methane

Pallavi Mungse, Govindachetty Saravanan,* Tomoki Uchiyama, Maiko Nishibori, Yasutake Teraoka, Sadhana Rayalu, and Nitin Labhsetwar *



Mixed oxides of Cu and Mn (CuMn₂O₄) showed stable, multi-cycle performance and CO₂-selectivity for chemical looping combustion reaction.